Composites Part B 215 (2021) 108751

Contents lists available at ScienceDirect

Composites Part B

journal homepage: www.elsevier.com/locate/compositesb

Tribological behaviors of novel epoxy nanocomposites filled with solvent-free ionic SiO_2 nanofluids

Yuexia Guo [a,b], Ligang Zhang [a,**], Fuyan Zhao [a], Guitao Li [a], Ga Zhang [a,b,c,*]

[a] State Key Laboratory of Solid Lubrication, Lanzhou Institute of Chemical Physics, Chinese Academy of Sciences, Lanzhou, 730000, China
[b] Center of Materials Science and Optoelectronics Engineering, University of Chinese Academy of Sciences, Beijing, 100049, China
[c] Qingdao Center of Resource Chemistry & New Materials, Qingdao, 266071, China

ARTICLE INFO

Keywords:
Nanofluids
Nanocomposite
Boundary lubrication
Tribofilm
Tribo-chemical reaction

ABSTRACT

A novel nanocomposite was prepared by uniformly dispersing synthesized solvent-free ionic SiO_2 nanofluids (NFs) into epoxy resin (EP). Tribological performance of SiO_2 NFs/EP composites were investigated when rubbing against bearing steel under base oil lubrication conditions. The results demonstrate that the addition of even low-loading SiO_2 NFs greatly improves the tribological performance of EP. It is disclosed that a nanostructured tribofilm grows on the steel surface when sliding against the EP nanocomposite filled with SiO_2 NFs. Comprehensive analyses of tribofilms' nanostructures suggest that tribofilm growth is fed by the molecular species released from the EP nanocomposite. Formation of the load-bearing tribofilm is surmised essential for the enhanced tribological performance of the EP nanocomposite. This work paves a good formulation route for developing high-performance tribo-composites subjected to harsh lubrication conditions.

1. Introduction

Operating environments of mechanical motion components become increasingly harsh with rapid development of modern transportation and other industrial activities [1,2]. Frequent start-stop and high load compel the motion components very often running under harsh mixed and even boundary lubrication conditions, resulting in excessive wear and even scuffing [3,4]. For certain applications under harsh lubrications conditions, the lifespan and reliability of conventional metal-metal sliding pairs can not meet the high requirements [5,6]. Thus, developing high-performance tribo-materials to replace traditional metal-metal ones are necessary for improving the anti-wear durability of the motion components.

Polymer-based composites have been increasingly utilized as self-lubricating materials by virtue of their superior tribological performance, high mechanical properties and corrosion resistance [7,8]. Important advances have been achieved in aspects of both tribology fundamentals and application developments of polymer self-lubricating materials over the past two decades. Numerous high-performance self-lubricating composites were formulated for different sliding contact conditions [9–11]. In particular, tribological behaviors and hindering mechanisms of polymer-based materials under dry sliding conditions were comprehensively investigated [12–14].

It has been identified that growth of a high-performance tribofilm is of importance for mitigating direct rubbing of the friction pairs subjected to mixed and boundary lubrication conditions [15–17]. Being different from dry friction, presence of lubricating oil at the interface can significantly hinder material transfer. Besides, in comparison to dry friction, tribo-physical and chemical actions occurring at the interface can be significantly restrained since the lubricating medium absorbs significant friction-induced heat [18,19]. As a consequence, tribofilm growth can be much suppressed due to presence of oil at the friction interface. Promoting growth of tribofilm may be a key factor for designing high-performance polymer composites for applications under oil lubrication conditions. Previous study has shown that addition of nanoparticles (NPs) into polymer matrix remarkably improves its friction-reduction and anti-wear performance [20–22]. The positive role is attributed to entrapment of NPs into the tribofilm which enhances its load-bearing capability [19,23]. However, conventional nanofillers were hard to disperse homogeneously owing to their strong agglomeration tendency and poor compatibility with polymer matrix [24,25]. Therefore, to uniformly disperse nanofillers into polymer matrix

* Corresponding author. State Key Laboratory of Solid Lubrication, Lanzhou Institute of Chemical Physics, Chinese Academy of Sciences, Lanzhou, 730000, China.
** Corresponding author.
E-mail addresses: zhanglg@licp.cas.cn (L. Zhang), gzhang@licp.cas.cn (G. Zhang).

https://doi.org/10.1016/j.compositesb.2021.108751
Received 4 December 2020; Received in revised form 23 February 2021; Accepted 23 February 2021
Available online 5 March 2021

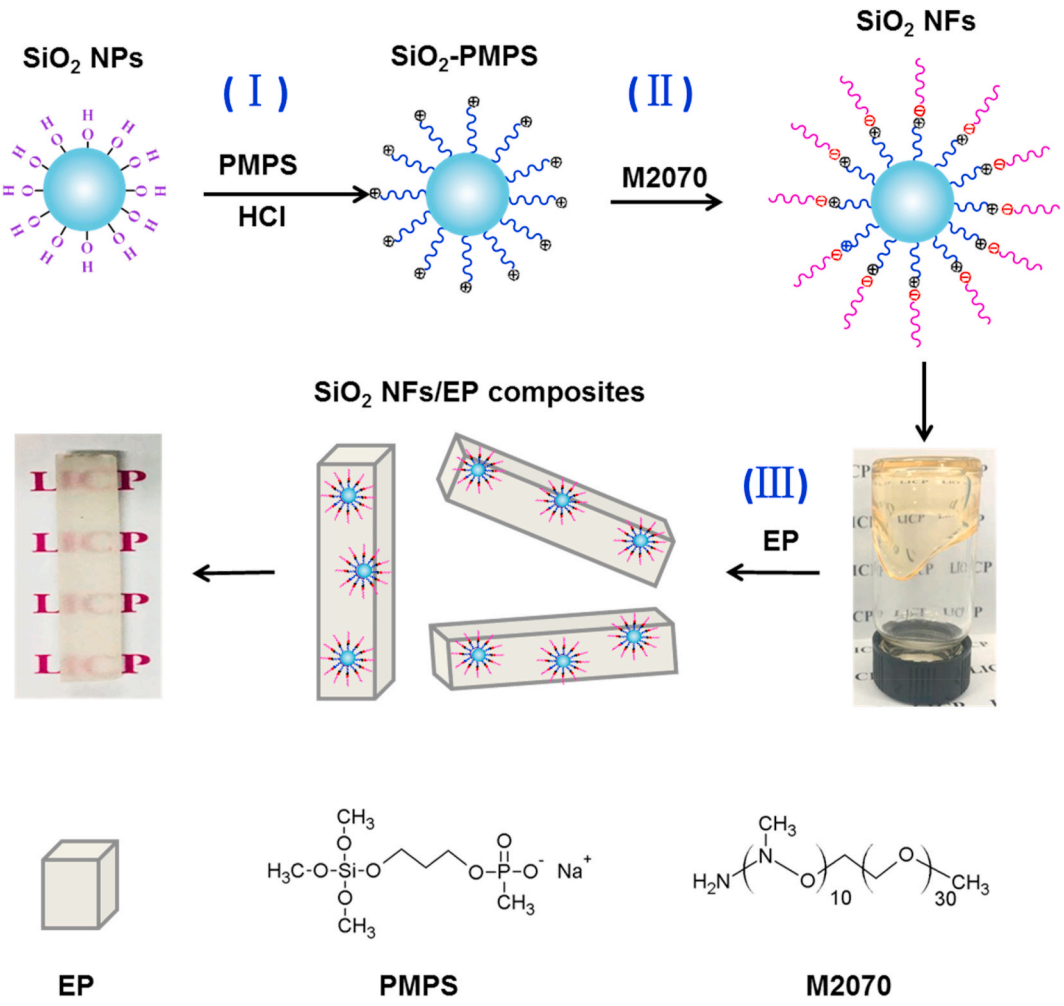

Scheme 1. Schematic synthetic procedures of SiO_2 NFs and SiO_2 NFs/EP composites.

dramatically remains a challenging task.

Recently, a novel organic-inorganic hybrid nanomaterial, solvent-free ionic nanofluids (NFs) was synthesized via grafting a soft organic shell onto NPs surface by covalent and ionic bonding. Existence of the special shell structure restrains efficiently strong agglomeration of NPs [26,27]. NFs show a liquid-like behavior at room temperature in absence of any solvent as well as superior dispersion stability in a variety of solvents [28,29]. More interestingly, NFs exhibit excellent lubricity when used as lubricant and additives of base oils, especially under extreme conditions [30–32]. Furthermore, NFs as nanofillers can be well dispersed in polymer matrices, e.g. epoxy resin (EP) and poly(vinyl chloride) [33–35]. It has been demonstrated that the mechanical properties of composites, such as flexural modulus, strength and impact toughness, are significantly improved due to addition of the NFs [36,37]. However, tribological behaviors of polymers reinforced with solvent-free ionic NFs have been rarely reported yet, which limits potential applications of NFs as functional fillers for developing high-performance tribo-materials.

In the present work, solvent-free ionic SiO_2 NFs were synthesized and tribological performance of EP filled with SiO_2 NFs was explored under oil lubrication conditions. Nanostructures of the tribofilms formed on the steel counterface and related tribo-chemical reactions were comprehensively characterized for gaining insight into the lubrication mechanisms. It is expected that output of this work can pave a route for developing novel polymer nanocomposites with excellent friction-reduction and anti-wear properties for applications subjected to harsh lubrication conditions.

2. Experimental

2.1. Materials

Ludox colloidal SiO_2 (Ludox-SM, 30 wt% suspension in H_2O, pH: 9.7–10.3) was purchased from SigmaAldrich Chemistry Co. 3(trihydroxysilyl)propyl methylphosphonate monosodium salt solution (50 wt % in H_2O) (PMPS) was obtained from Heowns OPDE Technologies. Amino-terminated block copolymer (Jeffamine M2070, molecular weight: ~2000) was supplied by Guangzhou Hengyu Trade Ltd. Bisphenol-A diglycidyl ether epoxy resin (EP, WSR618) with an epoxide equivalent weight of 182–192 g/equiv were obtained from Nantong Xingchen Synthetic Material Co., Ltd. Amine hardner triethylenetetramine (TETA) was supplied by Sinopharm Chemical Reagent Co., Ltd. Poly alpha olefins (PAO4) base oil was purchased from Exxon Mobil Corporation. All the chemicals were used as received without further purification.

2.2. Preparation of SiO_2 NFs and SiO_2 NFs/EP composites

Preparation of SiO_2 NFs: In the present work, SiO_2 NFs were synthesized via acid-base reaction. Organic corona PMPS and canopy layers M2070 were grafted onto the surface of SiO_2 nanocores via covalently functionalization and ionically tethering, following the route depicted in Scheme 1 (Step I and II). Ludox colloidal SiO_2 was diluted with deionized water with the assistance of sonication. Then, PMPS solution was slowly added into the above suspension for covalently grafting the

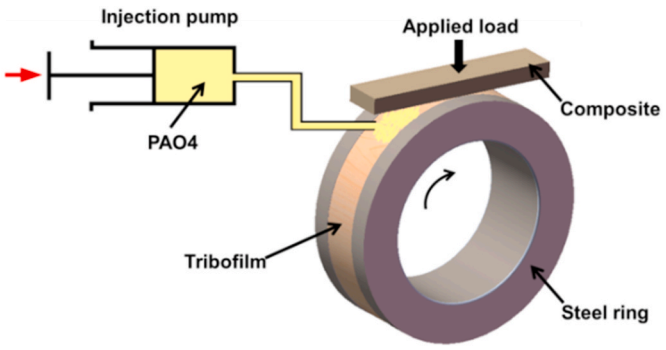

Scheme 2. Schematic illustration of the contact configuration of the POR tribological tests.

silanol groups with the hydroxyl groups on the surface of SiO_2 NPs. The reaction was performed at 70 °C for 24 h with vigorous stirring to completing the grafting process. Afterwards, the solvent was removed by centrifugation and the solid product was treated with strong acid for the purpose of replacing Na^+ with H^+. Subsequently, the aqueous solution of M2070 was dropwise added into functionalized SiO_2 NPs solution to neutralize all the phosphonate groups and ionically tether the canopy layer with the organic corona. The solvent-free SiO_2 NFs was obtained by washing repeatedly with deionized water and toluene to remove the excessive M2070, and then drying by vacuum drier. More details on SiO_2 NFs synthesis are available in our recent paper [38].

Preparation of the SiO_2 NFs/EP composites: As-prepared SiO_2 NFs was dispersed in 50 g EP and the contents of SiO_2 NFs varied from 0.5 wt % to 10 wt%. The mixture was vigorously stirred at a rotation speed of 6000 rpm for 15 min by using a high speed vacuum dissolver (Dispermat CN-10, VMA-Getzmann, Germany). After EP and SiO_2 NFs were mixed completely, the compounds were then blended with the TETA curing agent in the vacuum dissolver for 15 min. Finally, the mixture was poured into release agent-coated metallic molds and kept at room temperature for 2 h, followed by curing at 100 °C for 1 h and the SiO_2 NFs/EP composites were obtained. The detailed preparation of SiO_2 NFs/EP composites are illustrated in Scheme 1 (Step III). Besides, as reference materials, pure EP and EP filled with SiO_2 NPs composites were prepared in a similar way.

2.3. Characterizations of as-synthesized SiO_2 NFs and SiO_2 NFs/EP composites

High-Resolution Transmission Electron Microscopy (HR-TEM, Tecnai G^2 TF20, FEI) was employed to characterize the microscopic morphologies of SiO_2 NFs and the dispersion of SiO_2 NFs in epoxy matrix. Fourier Transform-Infrared Spectroscopy (FTIR, Nicolet 6700, Thermo Fisher Scientific) was conducted to analyze chemical structures of the SiO_2 NFs/EP composites.

2.4. Tribological tests

Tribological behaviors of the SiO_2 NFs/EP composites were evaluated using a MRH-1A tribometer (Jinan Yihua, China) with a plate-on-ring (POR) configuration following the standard ASTM G77-05. Schematic of the contact configuration of POR tribological tests is illustrated in Scheme 2. The composite plates have dimensions of 50 mm × 10 mm × 4 mm. The steel counterpart is bearing steel ring (GCr15, China GB/T 18254–2002) with a diameter of 60 mm and average roughness R_a of 0.1–0.2 μm. The polymer plates and the steel ring counterparts were ultrasonically cleaned thoroughly with petroleum ether before and after friction tests.

Two sets of tribological tests were conducted. First, to evaluate friction evolutions as a function of the speed and to deduce Strieback curves, tribological tests with stepwise increasing the speed from 0.05 to 0.5 m/s (each step 0.5 h) were performed. Second, to verify the role of SiO_2 NFs under a harsh lubrication condition, tribological performance of the EP-based materials at a constant low speed, i.e. 0.05 m/s, were compared. Duration of the tests at the constant speed was 3 h. The applied load was fixed at 300 N for both kinds of tests. 0.3 mL of poly alpha olefins (PAO4, SpetraSyn4, Mobil) base oil was pushed continuously onto the plate-ring contact zone with an injection rate of 0.1 mL/h by a high-precision microinjection pump (Baoding Lange Constant Flow Pump Co., Ltd., LSP02-1B, China). Friction coefficient is defined as the ratio of kinetic friction force (F) to the normal load applied and continuously recorded during the sliding process. Each test was repeated for at least three times. It is the objective of this work to explore the tribological property of the SiO_2 NFs/EP composites under boundary and mixed lubrication conditions. Lambda ratios (ratio of oil film thickness to comprehensive surface roughness) were investigated to confirm the lubrication regime of sliding system. The thickness of oil film at the sliding speed steps was calculated with the following Hamrock-Dowson formula [39]:

$$h_{min} = 3.63\,(\eta v/(ER))^{0.68}\,(\alpha E)^{0.49}\,(F/(ER^2))^{-0.073}\,(1\text{-}e^{-0.68k}) \quad (1)$$

Where h_{min} is the minimum oil film thickness of the contact surfaces (m), η is the dynamic viscosity of PAO4 base oil (N·s/m^2), v is the sliding speed (m/s), E is the comprehensive E-modulus of the tribo-pair (N/m^2), R the radius of the steel ring (m), αis the viscous pressure coefficient of PAO4 base oil (m^2/N), F is the normal applied load (N/m), k is a is a constant, k = 1.03.

The specific wear rate (W_s) was calculated according to the following formula:

$$W_s = L' \times \left(R^2 \arcsin\left(\frac{W}{2R}\right) - \frac{W}{4}\sqrt{4R^2 - W^2}\right) \Big/ FL \quad (2)$$

Where W_s is the specific wear rate (mm^3/Nm), L' and W are the length and width of the wear trace (mm), R corresponds to the radius of the counterpart ring (mm), and F is the normal load (N) applied during sliding, respectively. L represents the total sliding distance (m).

2.5. Characterization of worn surfaces and tribofilms

Morphologies of the worn surfaces were characterized using an Optic Microscope (Axio Imager A2m, Zeiss) and a Field Emission Scanning Electron Microscopy (FE-SEM, Merlin Compact, Carl Zeiss) instrumented with an Energy Dispersive X-ray Spectroscope (EDS, Energy 350, Oxford). Tribo-chemical reactions were analyzed using Raman Spectrometer, Attenuated Total Reflectance Fourier Transform Infrared Spectroscopy (ATR-FTIR, TENSOR 27 IFS120HR, Bruker) and a multifunctional X-ray Photoelectron Spectrometer (XPS, ESCALAB 250Xi, Thermo Fisher Scientific) with Al Kα radiation as the excitation source. Nanostructures of the tribofilms were characterized using the above HR-TEM. The slices of tribofilms' cross-sections were prepared by Focused Ion Beam (FIB) machining in a DualBeam SEM/FIB instrument (Quanta 3D FEG, FEI). The regions of interest were covered with a platinum cap layer before cutting cross-sectional lamellae to protect the boundary film.

3. Results and discussions

3.1. Characterization of the SiO_2 NFs and SiO_2 NFs/EP composites

Characterization results of the SiO_2 NFs, i.e. TEM graphs, FTIR, TGA curves and liquid behaviors of the SiO_2 NFs are given in our previous work [38]. The SiO_2 NFs show a stable dispersion without obvious agglomeration. FTIR analyses corroborate that SiO_2 NPs are successfully grafted with organic corona and canopy. From the TGA results, NFs exhibit an outstanding thermal stability. Importantly, SiO_2 NFs display

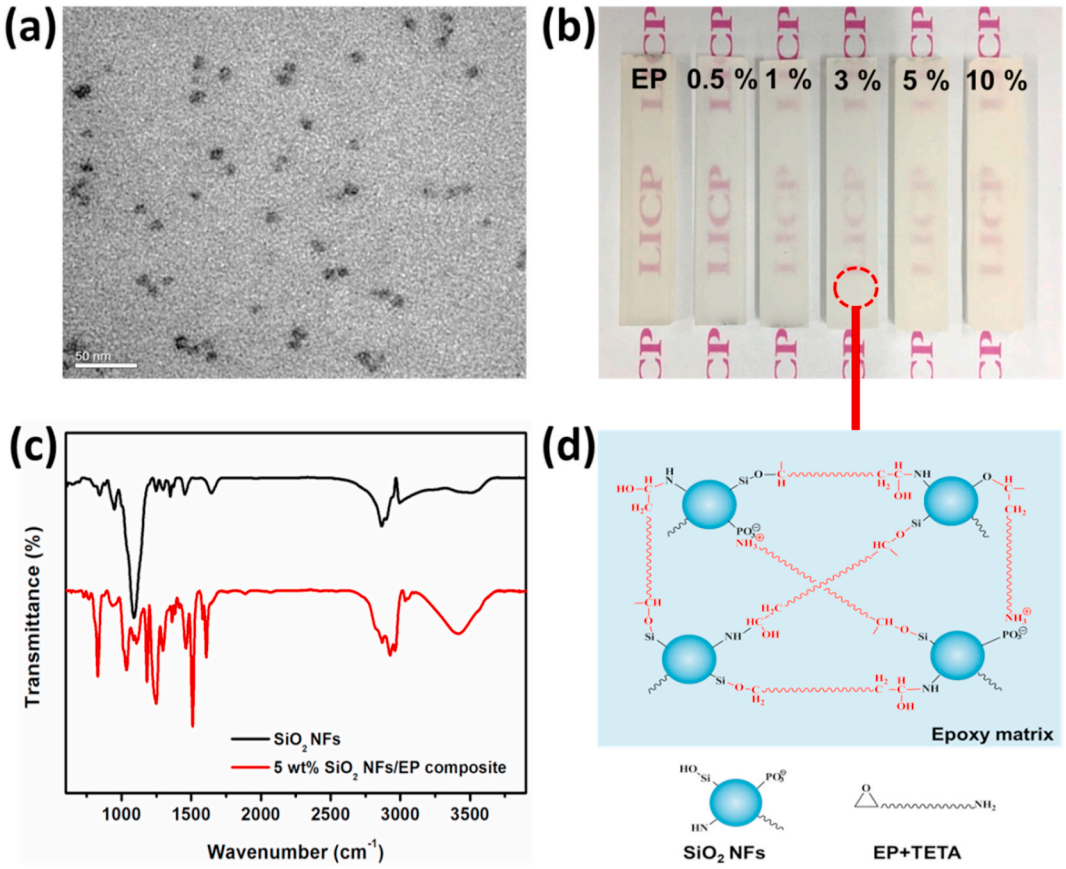

Fig. 1. (a) TEM micrograph of 1 wt% SiO_2 NFs/EP composite slice, (b) digital graphs of EP and SiO_2 NFs/EP composites, (c) FTIR spectra of SiO_2 NFs and 5 wt% SiO_2 NFs/EP composites, (d) Schematic illustration for the effect of SiO_2 NFs in EP matrix.

the property of a liquid material since the dynamical loss modulus G″ is apparently higher than the storage modulus G′ throughout the temperature range of 20–60 °C.

TEM was employed to investigate the dispersion of the SiO_2 NFs in EP matrix. As shown in Fig. 1a, SiO_2 NFs distribute uniformly in the EP matrix and severe agglomeration is not noticed, indicating the significant compatibility between SiO_2 NFs and EP, which is attributed to the long and flexible organic shell of SiO_2 NFs. On the one hand, the shell layer acts as a "solvent" and effectively hinders agglomeration of the NPs. On the other hand, the corona and canopy of SiO_2 NFs are rich in hydrogen bond and amino functional group that can react with EP and thus integrate with each other. Besides, photographs show that EP composites filled with different contents of SiO_2 NFs are homogeneous and transparent overall (cf. Fig. 1b). It provides evidence that grafting of the shell layers inhibits aggregation of the SiO_2 NFs and thus yields a stable system with EP.

Chemical structures of SiO_2 NFs/EP composites were characterized by ATR-FTIR spectroscopy. Fig. 1c compares the FTIR spectra of SiO_2 NFs and EP composite filled with 5 wt% SiO_2 NFs. For SiO_2 NFs/EP composite, the absorption peaks at 1611, 1514 cm^{-1} and 1240, 1185 cm^{-1} correspond to the C–C stretching vibration of the aromatic ring and C–O asymmetrical aromatic stretching vibration of EP [19,40]. In particular, new peaks appearing at 1105 and 812 cm^{-1} are assigned to the symmetrically stretching vibration of Si–O–Si that deriving from the SiO_2 NFs [41]. Compared to SiO_2 NFs, the peak at 3420 cm^{-1} (-OH stretching vibration) of SiO_2 NFs/EP composite exhibits strong signal due to the epoxy groups break to form more –OH [42]. Moreover, the new absorption peaks at 1194 and 1075 cm^{-1} are ascribed to Si–O–C stretching vibration that is not belonging to EP and SiO_2 NFs. This result suggests that –OH group from the breakage of epoxy group acts as a linker grafting EP with redundant Si–OH of SiO_2 NFs' corona layer, and thus the Si–O–C bonds are formed. As illustrated in Fig. 1d, it is believed that active functional groups and the nanosized property allow the SiO_2 NFs embed in the interspace of resin chains, and then via chemical bonds

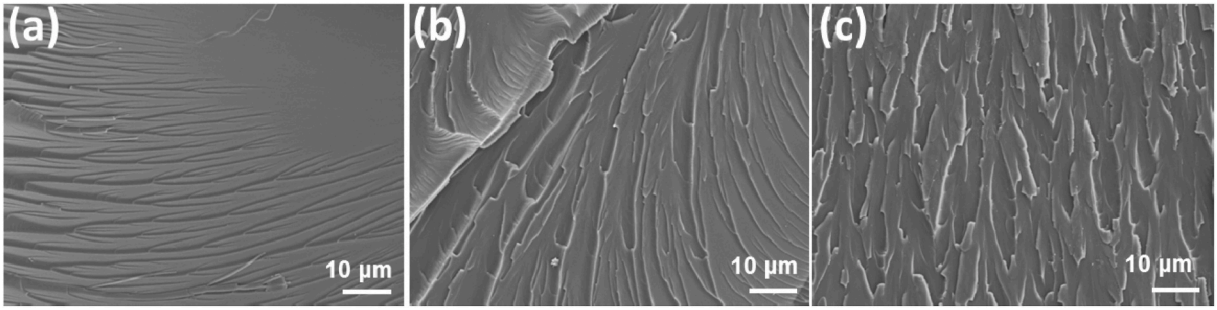

Fig. 2. SEM micrographs of the fracture surfaces of (a) EP, (b) 0.5 wt% SiO_2 NFs/EP and (c) 5 wt% SiO_2 NFs/EP composites.

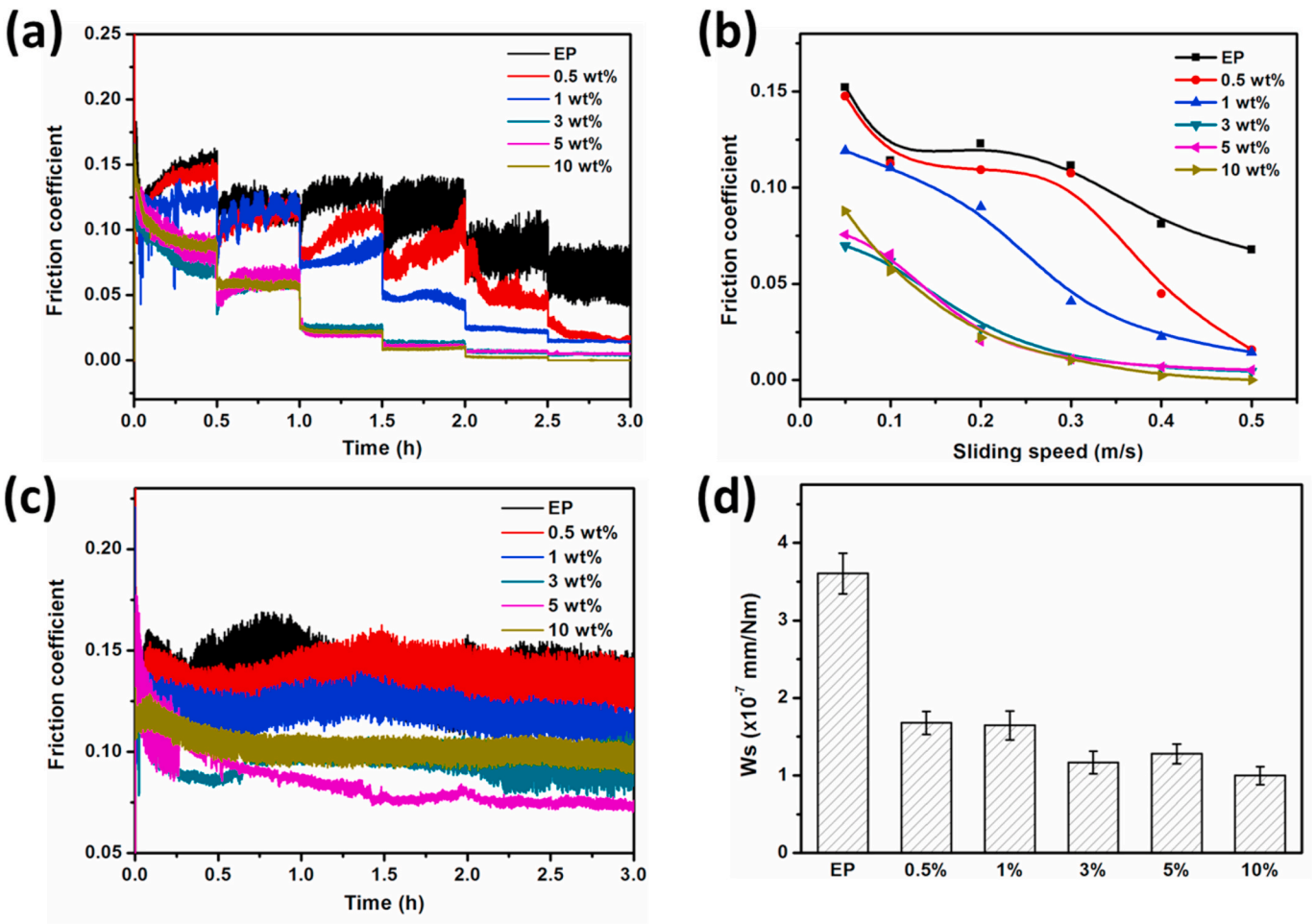

Fig. 3. (a) Friction coefficients as a function of sliding speed (0.05, 0.1, 0.2, 0.3, 0.4, 0.5 m/s) and sliding time of pure EP and SiO_2 NFs/EP composites; (b) Stribeck curves derived from average friction coefficients of EP and SiO_2 NFs/EP composites at each speed (0.05, 0.1, 0.2, 0.3, 0.4, 0.5 m/s); (c) Evolutions of friction coefficient and (d) wear rates of EP and SiO_2 NFs/EP composites at the sliding speed of 0.05 m/s.

to form an inorganic-organic hybrid network structure during the curing process [43]. The unique structure plays a key role in improving the interfacial interaction and compatibility of SiO_2 NFs and EP matrix.

Fracture graphs of pure EP and the composites filled with 0.5 wt% and 5 wt% SiO_2 NFs were inspected by SEM. As shown in Fig. 2a, the fracture graph of pure EP appears relatively smooth with some river lines. In contrast, much more and deeper river lines are noticed from the impact fracture surfaces of SiO_2 NFs/EP composites with the increasing contents of SiO_2 NFs (cf. Fig. 2b and c). When adding 5 wt% SiO_2 NFs, the fracture surface becomes crimp and disordered instead of longer line, indicating that there is a transfer from brittle fracture to plastic fracture. In this case, much impact energy is dissipated through these new sites of SiO_2 NFs in the composites [43]. That is, the distinct facture graphs give a hint that the composites can absorb more energy during the fracture process, probably leading to higher toughness [44].

3.2. *Tribological properties of SiO_2 NFs/EP composites*

Fig. 3a gives the friction coefficient evolutions as functions of sliding time and speed of pure EP and SiO_2 NFs/EP composites when sliding against the steel counterpart lubricated with PAO base oil. As calculated from the Hamrock-Dowson formula, when sliding takes place at 0.05 m/s, the Lamda ratio (λ) is 0.13, indicating that the friction pairs lie in the boundary lubrication regime. Stribeck curves of pure EP and SiO_2 NFs/EP composites were shown in Fig. 3b based on the average friction coefficients obtained from each speed step. The friction coefficients continuously decrease with increasing the speed to 0.5 m/s; it is thus inferred the friction pair shifts to the mixed lubrication regime. Under mixed lubrication conditions, the tribological behavior is determined by both lifting effect of the oil film but also by the materials themselves.

It is observed that the addition of even only 0.5 wt% SiO_2 NFs improved effectively the friction-reduction property of EP matrix throughout the sliding speed range of 0.05–0.5 m/s (0.05, 0.1, 0.2, 0.3, 0.4, 0.5 m/s). With increasing SiO_2 NFs content to 1–10 wt%, the tribological property of SiO_2 NFs/EP composites was further enhanced, illustrating the presence of SiO_2 NFs can significantly improve lubricity of the composites.

In order to verify the role of SiO_2 NFs under harsh boundary lubrication conditions, tribological tests at constant sliding speed of 0.05 m/s were conducted. Each test lasted 3 h. Fig. 3c compares friction coefficient evolutions of pure EP and EP composites filled with 0.5–10 wt% SiO_2 NFs. It is illustrated that pure EP has a longer running-in period than the composites reinforced with SiO_2 NFs. Increment of the SiO_2 NFs content from 0.5 to 5 wt% leads to continuous reduction of the friction coefficient. Nevertheless, further increasing the SiO_2 NFs from 5 to 10 wt% leads to slight increase of the friction coefficient. It is worth to note that the first 0.5 h sliding corresponding to the running-in stage and the friction coefficients have not stabilized yet. After the running-in stage, the nanocomposite containing 5 wt% SiO_2 NFs exhibits the lowest friction coefficient among the materials studied. The addition of SiO_2 NFs dramatically decreases the wear rate of EP, as seen from Fig. 3d. In comparison to pure EP, the wear rate of 3 wt% SiO_2 NFs/EP composite is

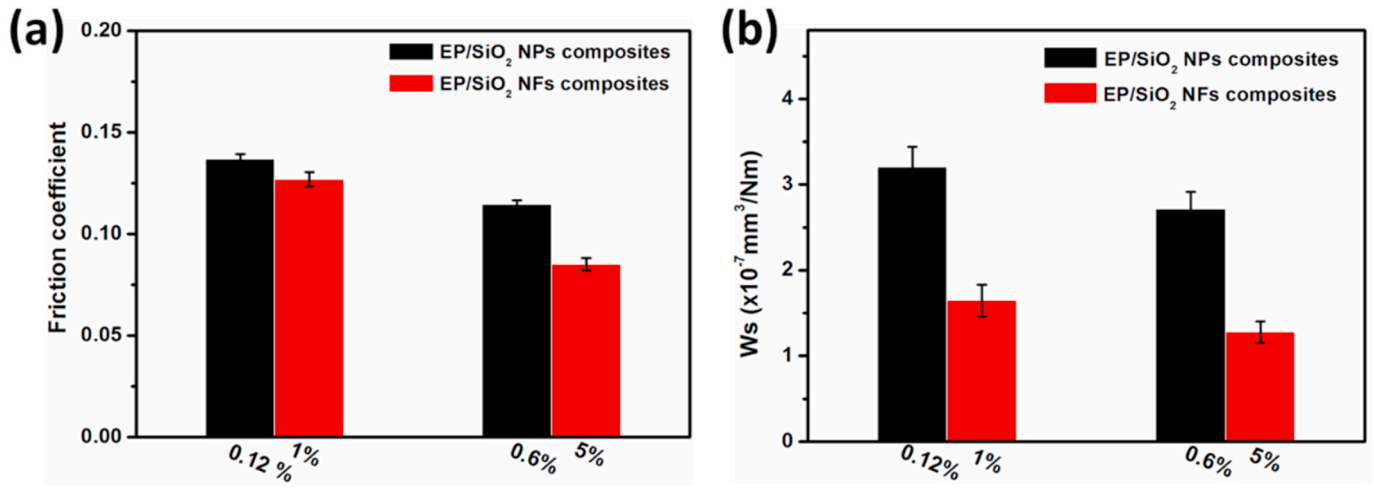

Fig. 4. (a) Friction coefficients and (b) wear rates of SiO_2 NFs/EP and SiO_2 NPs/EP composites with equivalent content of SiO_2 NPs at the sliding speed of 0.05 m/s.

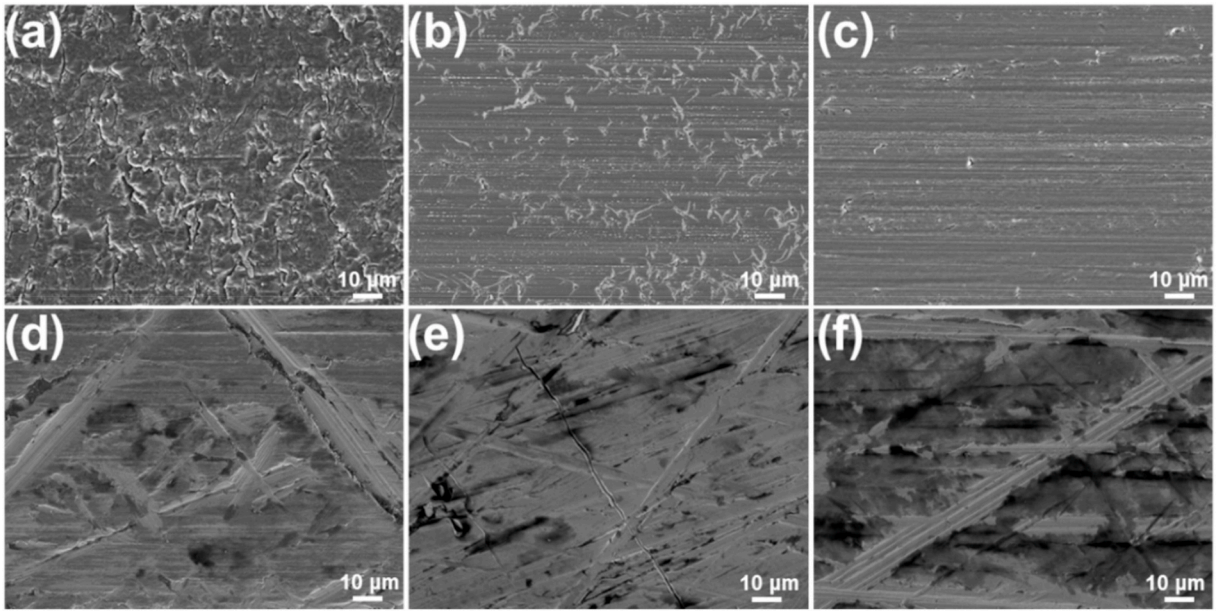

Fig. 5. SEM morphologies of worn surfaces of (a) pure EP, (b) 0.6 wt% SiO_2 NPs/EP and (c) 5 wt% SiO_2 NFs/EP composites. SEM morphologies of steel counterpart surfaces slid against (d) pure EP, (e) 0.6 wt% SiO_2 NPs/EP and (f) 5 wt% SiO_2 NFs/EP composites.

reduced by up to 67%. However, further increment of SiO_2 NFs content from 3 wt% to 10 wt% does not lead to significant change of the wear rate.

For sake to elucidate possible synergism of the NPs core and organic shell of SiO_2 NFs, tribological behaviors of SiO_2 NPs/EP and SiO_2 NFs/EP composites are compared under the same testing conditions. From the TGA results of SiO_2 NFs [38], the content of SiO_2 NPs in SiO_2 NFs is 12 wt%. In order to keep equivalent contents of SiO_2 core, EP composites reinforced with 0.12 and 0.6 wt% SiO_2 NPs were prepared, which contain the same fractions of SiO_2 cores as the EP composites reinforced with 1 and 5 wt% SiO_2 NFs. Fig. 4 shows the friction coefficients and wear rates of two kinds composites at the sliding speed of 0.05 m/s. It was seen that the friction and wear reduction achieved by blending SiO_2 NFs into EP matrix were superior to those achieved by adding SiO_2 NPs. We believe that such a unique core-shell structure of NFs make it possible to get the full lubrication potential of the inorganic NPs and organic soft shell.

Fig. 5 displays SEM micrographs of the worn surfaces of the EP-based materials and the steel counterparts. The worn surface of pure EP is rather rough with abundant micro-cracks perpendicular to the sliding direction (cf. Fig. 5a), which can be ascribed to adhesion between the sliding pair and fatigue of the EP matrix [8,45]. Interestingly, fewer cracks are noticed from the worn surface of EP filled with SiO_2 NPs (Fig. 5a and b). It seems that adhesion and fatigue wear of the EP matrix are suppressed due to addition of SiO_2 NPs. With respect to the worn surface of EP reinforced with SiO_2 NFs, almost no crack occurs and mild abrasion marks are noticed (Fig. 5c).

Fig. 5d–f compare the morphologies of steel counterpart surfaces slid against pure EP, SiO_2 NPs/EP and SiO_2 NFs/EP composites. Unlike the sliding of pure EP, the steel surfaces slid against the two kinds of composites show obviously less scratch destruction and are covered with patch-like tribofilms. The tribofilm filled the initial grooves and covered the plateau areas of the steel surface. Especially, a vast stretches of tribofilm were almost fully covered on the metal surface after rubbing with the SiO_2 NFs/EP composite. It is believed that the excellent tribological property of the SiO_2 NFs/EP composite is potentially ascribed to the formation of a robust tribofilm.

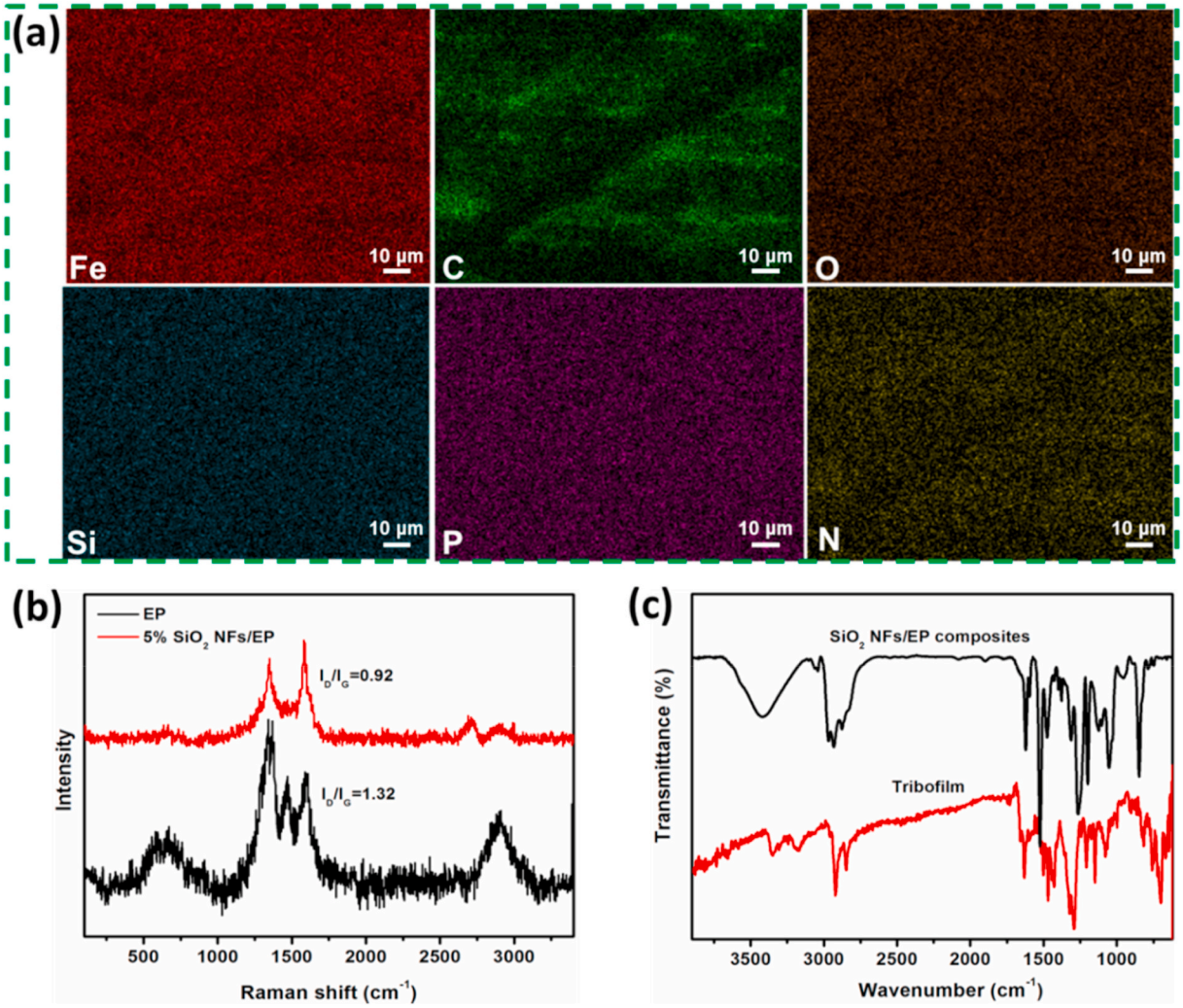

Fig. 6. (a) EDS elemental mapping of Fe, C, O, Si, P and N at the worn steel surface rubbed with pure EP and 5 wt% SiO_2 NFs/EP composite; (b) Raman spectra of the worn steel surface rubbed with pure EP and 5 wt% SiO_2 NFs/EP composite; (c) FTIR spectrum of SiO_2 NFs/EP composite and ATR-FTIR results of the steel worn surface rubbed with 5 wt% SiO_2 NFs/EP composite.

3.3. Characterizations of tribofilms and tribo-chemistry

It has been recognized that the formation of a high-performance tribofilm benefits to the improvement of the tribological properties of a composites in mixed and boundary lubrication regimes [19,46,47]. Fig. 6a gives the EDS elemental maps of steel worn surface after sliding with the 5 wt% SiO_2 NFs/EP composite. It is observed that besides Fe element from the steel substrate, C, O, Si, P and N elements are derived from SiO_2 NFs/EP composite also distribute evenly on the surface. From the Raman spectra of the steel surface after rubbing with pure EP, (cf. Fig. 6b), fingerprint of iron oxide at 670 cm^{-1} verifies that tribo-oxidation is occurred during the sliding process [48]. Nevertheless, the intensity of iron oxide on the steel surface after sliding with SiO_2 NFs/EP composite is much lower, indicating the tribo-oxidation was significantly inhibited. Besides, characteristic D band (1352 cm^{-1}) and G band (1605 cm^{-1}) of C element are present in the spectra of the steel surfaces after sliding with pure EP and 5 wt% SiO_2 NFs/EP composite, manifesting that carbon materials transferred onto the steel surface.

The intensity ratio of D band to G band (I_D/I_G) reflects the defect degree of carbon materials [49]. A higher intensity ratio of I_D/I_G refers to a relatively higher defect concentration. It can be reasonably inferred that the worn surface of steel sliding with the SiO_2 NFs/EP composite is covered with a more ordering carbon structure than that pure EP due to the lower I_D/I_G ratio (0.92 vs 1.32). Moreover, a new 2D-band (2680 cm^{-1}) appears on the steel surface rubbed with the SiO_2 NFs/EP composite, whereas such a peak is not observed from the spectra of worn surface rubbing with EP. The intensity of the S3-band (2910 cm^{-1}) is much lower when compares to the spectra of steel surface sliding against EP. This is another indication that tribofilm contains ordered structure carbon.

Fig. 6c compares the FTIR spectrum of SiO_2 NFs/EP composite and ATR-FTIR spectrum of the tribofilm formed on the steel surface after rubbed with 5 wt% SiO_2 NFs/EP composite. Characteristic absorption peaks of the respective chemical bonds of EP are identified from the spectrum of tribofilm. The absorption peaks at 1611 and 1514 cm^{-1} correspond to C–C stretching vibration of the aromatic ring. The peaks at 1240 and 1185 cm^{-1} are ascribed to the C–O asymmetrical aromatic stretching vibration. In addition, the peaks at 2920, 2871 and 1073 cm^{-1} become more obvious and stronger, which are assigned to the stretching vibration of $–CH_2$, $–CH_3$ and P═O that deriving from EP matrix and SiO_2 NFs, respectively. In particular, new absorption peaks of Si–OH bond and –OH are observed at 702 and 3180 cm^{-1}. It implies that SiO_2 NPs is released from SiO_2 NFs/EP composite and compacted into the tribofilm.

XPS analysis was used to characterize the chemical structures of the tribofilm that formed on the steel surfaces after rubbed with SiO_2 NFs/EP composite. As illustrated in Fig. 7, presence of iron oxide is verified by Fe2p peaks at 724.1 and 710.5 eV and O1s peak at 529.8 eV,

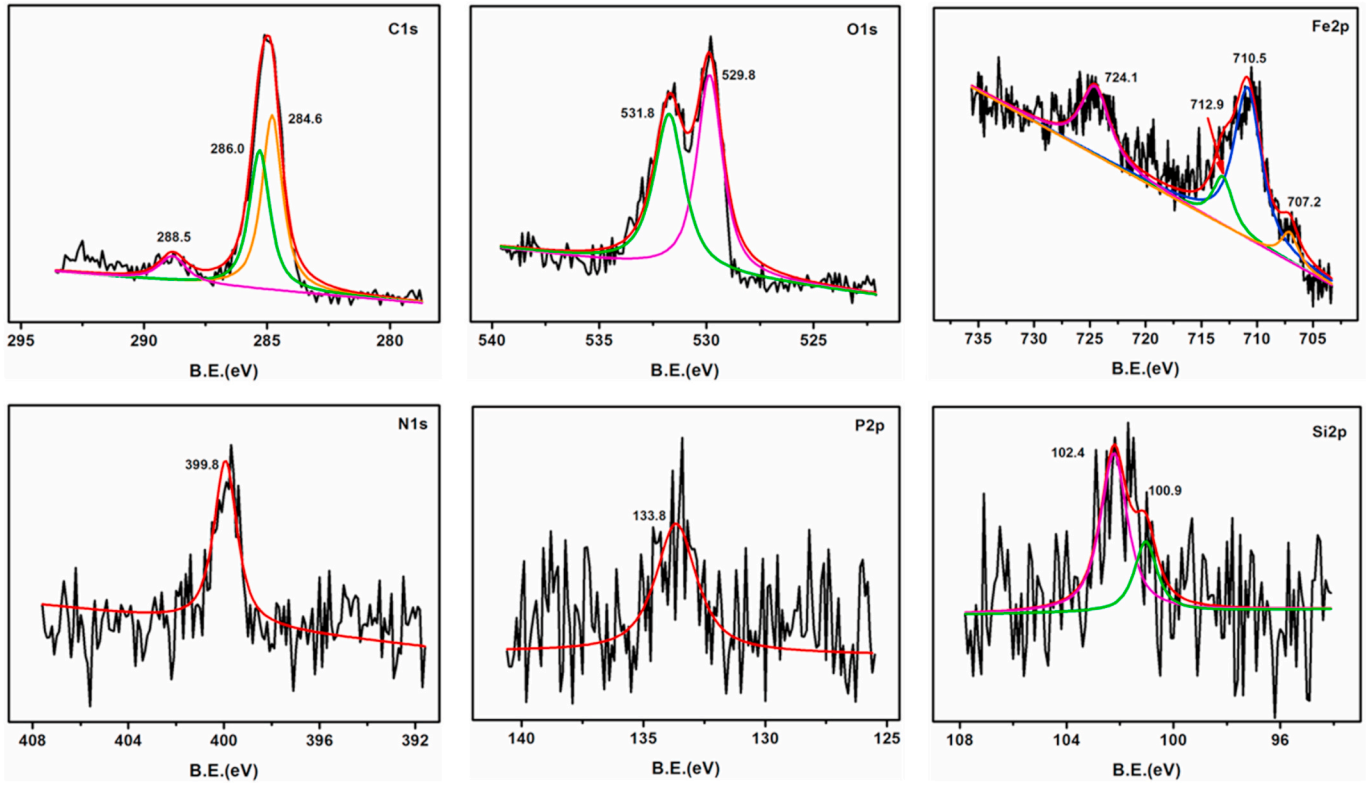

Fig. 7. XPS spectra of C 1s, O 1s, Fe 2p, N 1s, P 2p and Si 2p of the steel surface after rubbed with 5 wt% SiO_2 NFs/EP composite.

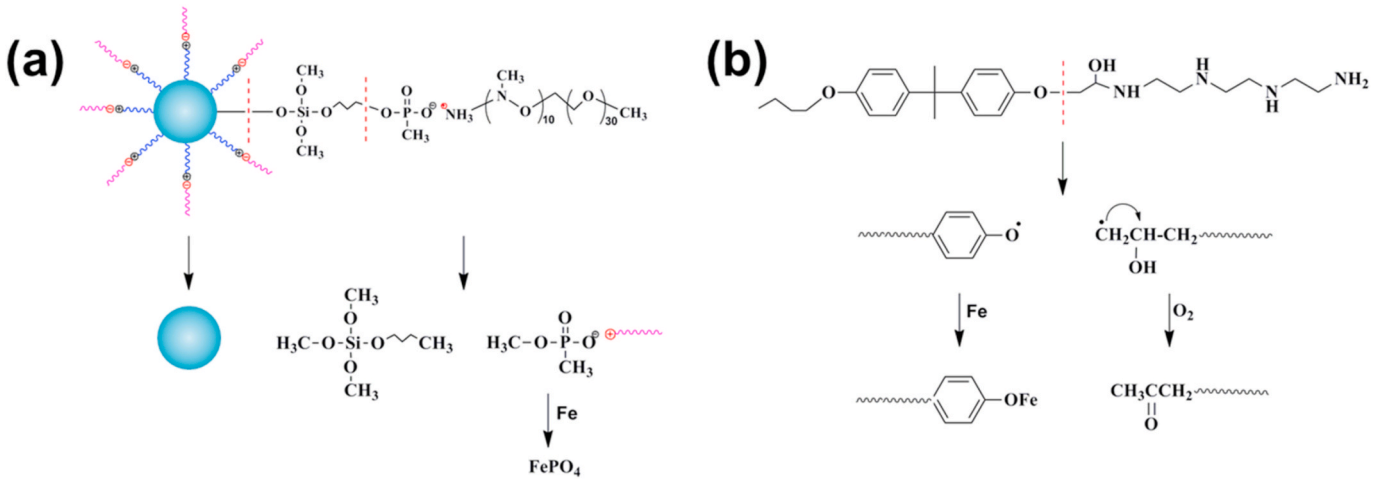

Scheme 3. (a) Breakage of solvent-free ionic SiO_2 NFs molecular chains and reaction of phosphonic acid group with metal ions of steel substrate; (b) breakage of bisphenol-A EP molecular chains, oxidation of the carbon free radicals and reaction of oxygen free radicals with metal ions of steel substrate.

indicating tribo-oxidation of the steel surface [50]. In addition, $FePO_4$ is generated in the tribofilm owing to the presence of characteristic peak at 712.8 eV in Fe2p spectrum and the peak at 133.8 eV in P2p spectrum [51]. Si2p peaks at 102.4 and 100.9 eV correspond to SiO_2 and methylsilane deriving from SiO_2 NFs. as shown in Scheme 3a, friction on interfaces tends to promote decomposition of SiO_2 NFs and react with steel substrate. Besides, the peak at 284.7 eV of C1s spectrum corresponds to C–C group from EP matrix and SiO_2 NFs. The peaks at 288.5 and 286.0 eV in C1s spectrum are likely assigned to C═O, C–N, respectively, as corroborated by the peak at 531.8 eV in O1s spectrum and the peak at 399.8 eV in N1s spectrum [52,53]. Moreover, the peak at 707.2 eV is assigned to ferrum-organic compounds producing from the tribo-chemical reaction [54]. As illustrated Scheme 3b, C–O bond in EP molecular chains are broken due to the highly interfacial stress and friction-heat. Then, the produced carbon free radicals are oxidized and C═O group is generated. Besides, the produced oxygen free radicals further react with the metal ions of the steel substrate, finally generating the ferrum-organic compounds [19]. Consequently, complex tribo-chemical actions of SiO_2 NFs and EP occur on the friction surface, promoting the growth of a resilient tribofilm.

For gaining insight into nanostructures of the tribofilms formed on the steel worn surface, FIB-TEM characterization was conducted. Fig. 8a provides direct evidence that a tribofilm with a thickness about 100 nm covers nearly the entire steel worn surface after rubbed with 5 wt% SiO_2 NFs/EP composite. It is observed that the tribofilm repairs the worn surface and separates effectively the direct rubbing of tribo-pairs.

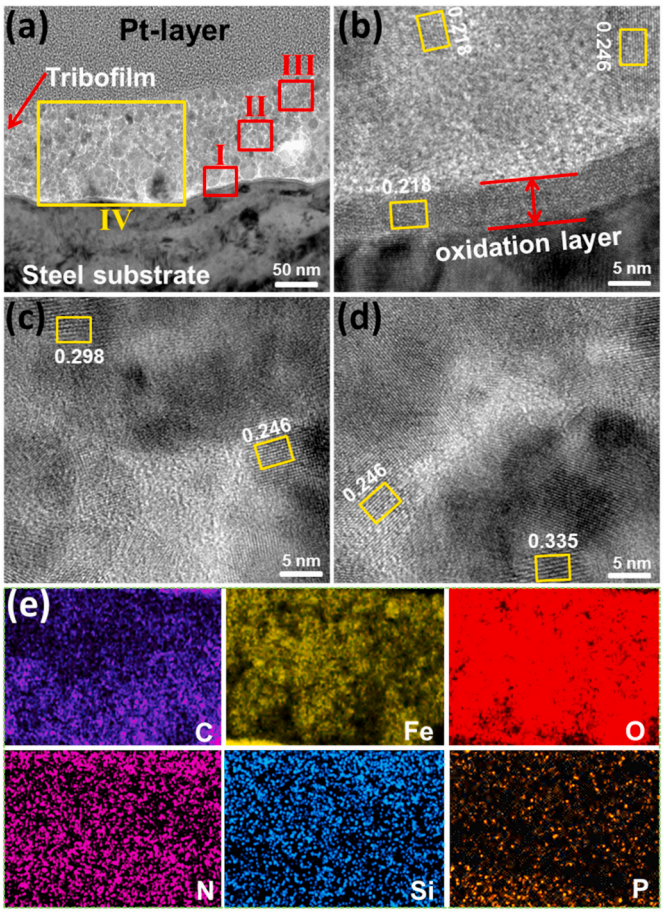

Fig. 8. (a) Overview of TEM micrograph of FIB-cut cross-section of the tribofilm formed on the steel ring after rubbed with 5 wt% SiO_2 NFs/EP composite; (b–d) HR-TEM micrographs of regions I-III indicated by the red squares in a; (e) EDS mapping of C, Fe, O, N, Si and P elements of region IV indicated by the yellow rectangle in a. (For interpretation of the references to colour in this figure legend, the reader is referred to the Web version of this article.)

HR-TEM observation of zone I as illustrated in Fig. 8b. It is revealed that a thin and continuous oxidation layer having a thickness of 5 nm firmly attaches to the steel substrate, consisting of Fe_2O_3 nanocrystals with lattice spacing of 0.218 nm. This gives a hint that tribo-oxidation of the steel counterface occurred due to the direct sliding of tribo-pair prior to the tribofilm formation. Oxidation layer plays a key role in jointing the bottom steel substrate and the upper tribofilm. As seen from Fig. 8c and d, the tribofilm above the oxidation layer is a mixture of amorphous phase and complex crystals. Close inspections disclose that some Fe_2O_3 nanocrystals with lattice spacing 0.298 and 0.246 nm are distributed in the amorphous matrix (cf. Fig. 8b and c). As shown in EDS mapping (cf. Fig. 8e), the tribofilm comprises abundant C, N elements and significant fractions of Si and P elements. Moreover, Fe and O elements are observed in the upper tribofilm, indicating that certain iron oxide crystals are abraded from the oxidation layer and consequently compacted into the tribofilm.

More interesting, a little short-range ordered graphite carbon with lattice spacing of 0.335 nm appears in the tribofilm (cf. Fig. 8d), potentially deriving from the polymer transfer. It is inferred that graphitization of the transferred polymer can be induced by the high stress and friction-heat, resulting in generation of partially ordered structures [52,55]. Meanwhile, the presence of Si, N and P elements indicates that SiO_2 NFs were decomposed and compacted into the tribofilm. The amorphous phase of tribofilm mainly consists of transferred polymer, SiO_2 NFs and some tribo-chemistry products, e.g. metallic organics, SiO_2 NPs. The complex mixture digested in the tribofilm can improve its easy-to-shear characteristic and load-carrying capability.

In summary, solvent-free ionic SiO_2 NFs exhibit excellent boundary lubrication performance while as reinforcement for EP-based materials. It is believed that a nanostructured protective tribofilm formed on the sliding steel surface due to complex tribo-physical and chemical actions. SiO_2 NFs and EP provide active molecular species and react with the metal surface, inducing the formation of tribofilm. In particular, transferred polymers, graphitized carbon and SiO_2 NPs constantly fed into the friction interface accelerate tribofilm growth and enhance its lubricity.

4. Conclusions

In this work, solvent-free ionic SiO_2 NFs were synthesized and dispersed uniformly into EP matrix for developing high-performance tribo-composites subjected to boundary lubrication conditions. Tribological behaviors of the NFs/EP composite were comprehensively investigated. Following conclusions can be drawn:

(1) SiO_2 NFs exhibit an excellent dispersibility in the EP matrix. Novel NFs/EP composite showed excellent tribological performance under boundary and mixed lubrication conditions. Adding even small amount of SiO_2 NFs into EP greatly reduces the friction and wear.
(2) It is disclosed that a nanostructured tribofilm grows on the steel surface when sliding against the EP nanocomposite filled with SiO_2 NFs. Tribofilm growing on the steel surface were comprehensively characterized. It was revealed that tribo-chemical reactions between the NFs-reinforced EP composites and steel counterface benefit tribofilm growth. Involvement of graphitized carbon, SiO_2 NPs and other tribo-chemical products in the tribofilm can enhances its load-carrying capability and shearing property.
(3) Output of this work shows that adding solvent-free NFs into EP resin specially provides an efficient route to improve wear resistance and friction-reduction performance of resin-based composites.

CRediT authorship contribution statement

Yuexia Guo: Conceptualization, Methodology, Software, Investigation, Writing – original draft. **Ligang Zhang:** Conceptualization, Validation, Writing – review & editing. **Fuyan Zhao:** Resources, Supervision, Writing – review & editing, Writing - review. **Guitao Li:** Supervision, Software. **Ga Zhang:** Writing – review & editing, Experiments: mentor. All authors read and contributed to the manuscript.

Declaration of competing interest

The authors declare that they have no known competing financial interests or personal relationships that could have appeared to influence the work reported in this paper.

Acknowledgments

The authors are grateful for financial support from National Key Research and Development Program of China (Grant number 2018YFE0119300) and the National Natural Science Foundation of China (Grant numbers 51875552, 51705505).

References

[1] Berman D, Erdemir A, Sumant AV. Approaches for achieving superlubricity in two-dimensional materials. ACS Nano 2018;12(3):2122–37.
[2] Berman D, Deshmukh SAD, Sankaranarayanan SKRS, Erdemir A, Sumant AV. Macroscale superlubricity enabled by graphene nanoscroll formation. Science 2015;348(6239):1118–22.

[3] Chen XC, Li JJ. Superlubricity of carbon nanostructures. Carbon 2020;158:1–23.
[4] Hod O, Meyer E, Zheng Q, Urbakh M. Structural superlubricity and ultralow friction across the length scales. Nature 2018;563(7732):485–92.
[5] Scherge M, Kramlich J, Böttcher R, Hoppe T. Running-in due to material transfer of lubricated steel/PA46 (aliphatic polyamide) contacts. Wear 2013;301(1–2):758–62.
[6] Xu YK, Qi HM, Li GT, Guo XP, Wan Y, Zhang G. Significance of an in-situ generated boundary film on tribocorrosion behavior of polymer-metal sliding pair. J Colloid Interface Sci 2018;518:263–76.
[7] Li YL, Wang Q, Wang SJ. A review on enhancement of mechanical and tribological properties of polymer composites reinforced by carbon nanotubes and graphene sheet: molecular dynamics simulations. Compos B Eng 2019;160:348–61.
[8] Myshkin N, Kovalev A. Adhesion and surface forces in polymer tribology-a review. Friction 2018;6(2):143–55.
[9] Yamamoto YJ, Takashima T. Friction and wear of water lubricated PEEK and PPS sliding contacts. Wear 2002;253:820–6.
[10] Jozwik J, Dziedzic K, Barszcz M, Pashechko M. Analysis and comparative assessment of basic tribological properties of selected polymer composites. Materials 2019;13(1).
[11] Zhang H, Wang LB, Chen Q, Li P, Zhou AG, Cao XX, Hu QK. Preparation, mechanical and anti-friction performance of MXene/polymer composites. Mater Des 2016;92:682–9.
[12] Upadhyay RK, Kumar A. Epoxy-graphene-MoS_2 composites with improved tribological behavior under dry sliding contact. Tribol Int 2019;130:106–18.
[13] Che QL, Zhang G, Zhang LG, Qi HM, Li GT, Zhang C, Guo F. Switching brake materials to extremely wear-resistant self-lubrication materials via tuning interface nanostructures. ACS Appl Mater Interfaces 2018;10(22):19173–81.
[14] Nunez EE, Polycarpou AA. The effect of surface roughness on the transfer of polymer films under unlubricated testing conditions. Wear 2015;326–327:74–83.
[15] Erdemir A, Ramirez G, Eryilmaz OL, Narayanan B, Liao Y, Kamath G, Sankaranarayanan SKRS. Carbon-based tribofilms from lubricating oils. Nature 2016;536(7614):67–71.
[16] Gosvami NN, Bares JA, Mangolini F, Konicek AR, Yablon DG, Carpick RW. Mechanisms of antiwear tribofilm growth revealed in situ by single-asperity sliding contacts. Science 2015;348(6230):102–6.
[17] Bahadur S. The development of transfer layers and their role in polymer tribology. Wear 2000;245:92–9.
[18] Cai MR, Yu QL, Liu WM, Zhou F. Ionic liquid lubricants: when chemistry meets tribology. Chem Soc Rev 2020;49(21):7753–818.
[19] Guo LH, Li GT, Guo YX, Zhao FY, Zhang LG, Wang C, Zhang G. Extraordinarily low friction and wear of epoxy-metal sliding pairs lubricated with ultra-low sulfur diesel. ACS Sustainable Chem Eng 2018;6:15781–90.
[20] Park MS, Sung HS, Park CH, Han TS, Kim JH. High tribology performance of Poly (vinylidene fluoride) composites based on three-dimensional mesoporous magnesium oxide nanosheets. Compos B Eng 2019;163:224–35.
[21] Xu X, Su FH, Li ZJ. Microstructure and tribological behaviors of Mon-Cu nanocomposite coatings sliding against Si_3N_4 ball under dry and oil-lubricated conditions. Wear 2019;434–435:202994.
[22] Samad MA, Sinha SK. Dry sliding and boundary lubrication performance of a UHMWPE/CNTs nanocomposite coating on steel substrates at elevated temperatures. Wear 2011;270(5–6):395–402.
[23] Bazrgari D, Moztarzadeh F, Sabbagh-Alvani AA, Rasoulianboroujeni M, Tahriri M, Tayebi L. Mechanical properties and tribological performance of epoxy/Al_2O_3 nanocomposite. Ceram Int 2018;44(1):1220–4.
[24] Chatterjee A, Islam MS. Fabrication and characterization of TiO_2-epoxy nanocomposite. Mater Sci Eng 2008;487(1–2):574–85.
[25] Jin FL, Park SJ. A review of the preparation and properties of carbon nanotubes-reinforced polymer compositess. Carbon 2011;12(2):57–69.
[26] Bourlinos AB, Herrera R, Chalkias N, Jiang DD, Zhang Q, Archer LA, Giannelis EP. Surface-functionalized nanoparticles with liquid-like behavior. Adv Mater 2005;17(2):234–7.
[27] Li Q, Dong LJ, Deng W, Zhu QM, Liu Y, Xiong CX. Solvent-free fluids based on rhombohedral nanoparticles of calcium carbonate. J Am Chem Soc 2009;131:9148–9.
[28] Peplow M. Nanoparticles go with the flow. Nature 2004;432:688.
[29] Nugent JL, Moganty SS, Archer LA. Nanoscale organic hybrid electrolytes. Adv Mater 2010;22(33):3677–80.
[30] Kim D, Archer LA. Nanoscale organic-inorganic hybrid lubricants. Langmuir 2011;27(6):3083–94.
[31] Yang J, Xia YF, Song HJ, Chen BB, Zhang ZZ. Synthesis of the liquid-like graphene with excellent tribological properties. Tribol Int 2017;105:118–24.
[32] Fernandes NJ, Akbarzadeh J, Peterlik H, Giannelis EP. Synthesis and properties of highly dispersed ionic silica poly(ethylene oxide) nanohybrids. ACS Nano 2013;7(2):1265–71.
[33] Liu H, Dong LJ, Xie HA, Wan LP, Liu ZK, Xiong CX. Ultraviolet light aging properties of PVC/$CaCO_3$ composites. J Appl Polym Sci 2013;127(4):2749–56.
[34] Fernandes NJ, Wallin TJ, Vaia RA, Koerner H, Giannelis EP. Nanoscale ionic materials. Chem Mater 2014;26(1):84–96.
[35] Li PP, Zheng YP, Shi T, Wang YD, Li MZ, Chen C, Zhang JA. solvent-free graphene oxide nanoribbon colloid as filler phase for epoxy-matrix composites with enhanced mechanical, thermal and tribological performance. Carbon 2016;96:40–8.
[36] Texter J, Qiu ZM, Crombez R, Shen WD. Nanofluid polyurethane/polyurea resins-thin films and clearcoats. J Polym Sci Polym Chem 2013;51:3439–48.
[37] Li Q, Dong LJ, Li L, Su XH, Xie HA, Xiong CX. The effect of the addition of carbon nanotube fluids to a polymeric matrix to produce simultaneous reinforcement and plasticization. Carbon 2012;50(5):2056–60.
[38] Du GH, Liu ZL, Xia X, Chu Q, Zhang SM. Characterization and application of Fe_3O_4/SiO_2 nanocomposites. J Sol Gel Sci Technol 2006;39(3):285–91.
[39] Hamrock BJ, Dowson D. Isothermal elastohydrodynamic lubrication of point contacts Part III-fully flooded results. Journal of Lubrication Technology 1977;99:264–75.
[40] Sanes J, Saurín N, Carrión FJ, Ojados G, Bermúdez MD. Synergy between single-walled carbon nanotubes and ionic liquid in epoxy resin nanocomposites. Compos B Eng 2016;105:149–59.
[41] Fidalgo A, Ilharco LM. The defect structure of solgel-derived silica/polytetrahydrofuran hybridlms by FTIR. J Non-Cryst Solids 2001;283:144–54.
[42] Lan L, Zheng YP, Zhang AB, Zhang JX, Wang N. Study of ionic solvent-free carbon nanotube nanofluids and its composites with epoxy matrix. J Nanoparticle Res 2012;14(3).
[43] Bai HP, Zheng YP, Yang RL, Zhang AB, Wang N. Thermal and mechanical properties of liquid-like trisilanol isobutyl-polyhedral oligomeric silsesquioxanes (POSS) derivative/epoxy nanocomposites. Polym Compos 2017;38(4):691–8.
[44] Rakesh S, Dharan CPS, Selladurai M, Sudha V, Sundararajan PR, Sarojadevi M. Thermal and mechanical properties of POSS-cyanate ester/epoxy nanocomposites. High Perform Polym 2012;25(1):87–96.
[45] Myshkin NK, Petrokovets MI, Kovalev AV. Tribology of polymers: adhesion, friction, wear, and mass-transfer. Tribol Int 2005;38(11–12):910–21.
[46] Lin LY, Schlarb AK. The roles of rigid particles on the friction and wear behavior of short carbon fiber reinforced PBT hybrid materials in the absence of solid lubricants. Tribol Int 2018;119:404–10.
[47] Hsu SM, Gates RS. Boundary lubricating films: formation and lubrication mechanism. Tribol Int 2005;38(3):305–12.
[48] Chourpa I, Douziech-Eyrolles L, Ngaboni-Okassa L, Fouquenet JF, Cohen-Jonathan S, Souce M, Marchais H, Dubois P. Molecular composition of iron oxide nanoparticles, precursors for magnetic drug targeting, as characterized by confocal Raman microspectroscopy. Analyst 2005;130(10):1395–403.
[49] Zhao J, Mao JY, Li YR, He YY, Luo JB. Friction-induced nano-structural evolution of graphene as a lubrication additive. Appl Surf Sci 2018;434:21–7.
[50] Espinosa T, Sanes J, Bermudez MD. New alkylether-thiazolium room-temperature ionic liquid lubricants: surface interactions and tribological performance. ACS Appl Mater Interfaces 2016;8(28):18631–86319.
[51] Weng LJ, Liu XQ, Liang YM, Xue QJ. Effect of tetraalkylphosphonium based ionic liquids as lubricants on the tribological performance of a steel-on-steel system. Tribol Lett 2006;26(1):11–7.
[52] Zhao FY, Zhang LG, Li GT, Guo YX, Qi HM, Zhang G. Significantly enhancing tribological performance of epoxy by filling with ionic liquid functionalized graphene oxide. Carbon 2018;136:309–19.
[53] Naumkin AV, Kraut-Vass A, Gaarenstroom SW, Powell CJ. NIST X-ray photoelectron spectroscopy (XPS) database. http://srdata.nist.gov/xps/. Accessed 28 July 2016.
[54] Guo YX, Guo LH, Li GT, Zhang LG, Zhao FY, Wang C, Zhang G. Solvent-free ionic nanofluids based on graphene oxide-silica hybrid as high-performance lubricating additive. Appl Surf Sci 2019;471:482–93.
[55] Wang YF, Gao KX, Zhang B, Wang Q, Zhang JY. Structure effects of sp_2-rich carbon films under super-low friction contact. Carbon 2018;137:49–56.